Babcock & Wilcox
Research and Development Division
Alliance Research Center Alliance, Ohio 44601

To	K. E. MOORE - TECHNICAL STAFF, NPGD, LYNCHBURG
From	L. W. SARVER/J. S. ROVDER - METALLURGY SECTION, ARC
Cust.	METROPOLITAN EDISON
File No. or Ref.	LR:77:5276-01:2
Subj.	FINAL REPORT ON EXAMINATION OF CR-3 DECAY HEAT PUMP SHAFT
Date	SEPTEMBER 24, 1977

This letter to cover one customer and one subject only

INTRODUCTION

This report describes the metallurgical evaluation and failure analysis of a broken CR-3 decay heat pump shaft. This failure occurred last year at the Crystal River N.S.S. facility of the Florida Power Corporation. The decay heat pump shaft was fabricated by the Worthington Pump Corp. from 17-4 PH stainless steel.

It is our understanding that similar equipment from Worthington was installed in other N.S.S. units at about the same time. At issue is whether other sites may face the potential of a decay heat pump shaft failure.

The purpose of this failure analysis is to attempt to identify any material problems or pump design problems which may have caused or contributed to this failure and, therefore, would raise questions about similar equipment at other sites.

CONCLUSIONS

The 17-4 PH stainless steel decay heat pump shaft appears to have failed by a fatigue mechanism. It appears that a non-filleted keyway design contributed substantially to the failure through a stress concentration effect. Further, it appears the material was not carefully heat treated (adequately tempered) to the specified condition and thus was placed in service in a more brittle and less fatigue resistant condition than intended for the application. It seems probable

---

Distribution (COMPANY LIMITED) This information is freely available to all Company personnel. Written approval by sponsoring unit's R&D coordinator is required only if release outside of the Company is requested.

P.S. Ayres - ARC
R.U. Blaser - ARC
D.F. Levstek - NPGD
E.L. Logan - NPGD
G. Musat - ARC
J.D. Phinney - NPGD
H.S. Swenson - ARC
Library (3) - ARC
Metallurgy File

1589 115

7910310 704

that this failure would not have occurred if a filleted keyway design had been used and if the shaft had been properly heat-treated.

RESULTS

MATERIAL CHARACTERISTICS

Chemical Composition

Element	Emission Spectrographic Chemical Analysis of Failed Shaft Wt. %	Wet-Chemical Analysis of Failed Shaft Wt. %	Certification Chemical Analysis Wt. %	ASTM A564 Grade 630 Chemistry Specified for 17-4 PH Stainless Steel Wt. %
C	.04	.05	.043	.07 Max
Mn	.36	.35	.31	1.00 Max
P	.012	.013	.017	.04 Max
S	.012	.011	.012	.03 Max
Si	.65	.67	.60	1.0 Max
Cr	15.8	15.8	15.90	15.5-17.5
Ni	4.6	4.5	4.36	3.0- 5.0
Mo	.11			
Cu	3.6			
V	.02			
Al	<.01			
Ti	<.01			
Co	.05			
Cb	.29	} .40		} 0.15-0.45
Ta	.01			

TENSILE TEST DATA

		Ultimate Tensile Stress (psi)	0.2% Yield Stress (psi)	% Elongation (0.8 inches)	%Reduction of Area
Shaft Specimens With Fracture Plane Perpendicular of Shaft Axis (Longitudinal)	1	161,000	160,000	15.0	54.6
	2	161,000	160,000	13.8	52.7
Shaft Specimens With Fracture Plane Parallel to Shaft Axis (Transverse)	1	158,000	153,000	7.5	14.7
	2	157,000	154,000	7.5	14.7
Typical H-1150 Properties					
Longitudinal		147,000	139,000	20	63
Transverse		147,000	136,000	15	44
Typical H-1025 Properties					
Longitudinal		163,000	160,000	17	58
Transverse		162,000	159,000	13	32

HARDNESS DATA

Schematics shown below illustrate the distribution of hardness values on transverse and longitudinal cross-sections of the shaft and in the corner of the keyway. The transverse cut was located about 1-1/2 to 2-1/2 inches from the seapration towards the thread end of the shaft. The longitudinal cut was taken from a sleeved portion of the shaft.

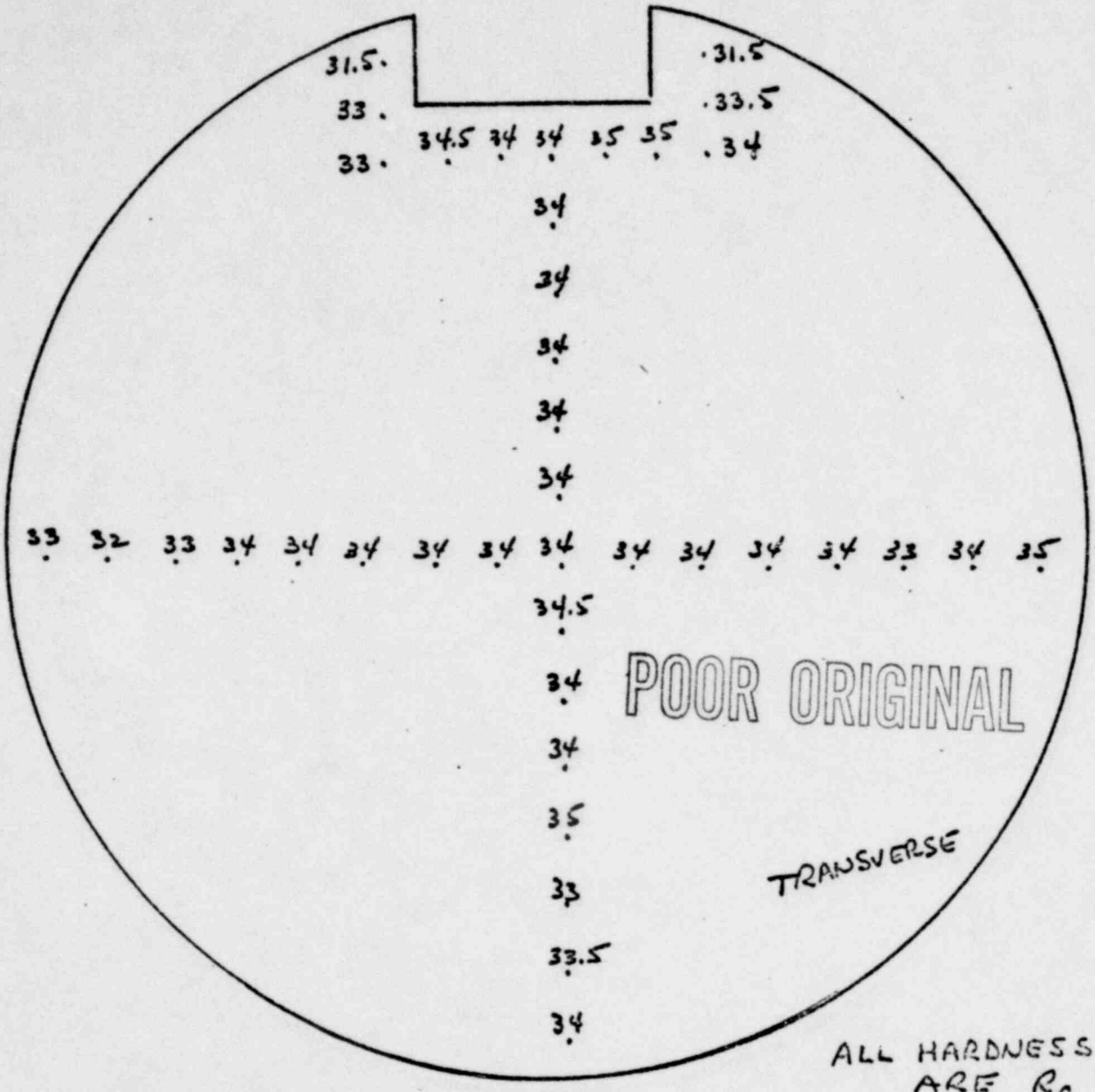

ALL HARDNESS VALUES ARE Rc

LOCATED $1\frac{1}{2}$ - $2\frac{1}{2}$" FROM THE FRACTURE.	.35
	.34
THIS IS PART OF THE SHAFT FROM IN THE PRESS FIT AREA	.35
	.35
	.35
	.35
	.35
	.35

LONGITUDINAL

MICROSTRUCTURE

The shaft microstructure consists predominantly of tempered martensite. Minor quantities of delta-ferrite and columbium-containing inclusion stringers are also present. Fine particulates of copper are dispersed throughout the microstructure. Prior austenite grain boundaries (~ASTM 2-3 grain size) are delineated by copper particles. Microstructures are illustrated in Figures 1-4.

FAILURE CHARACTERISTICS

Cracking occurred at and around the location where the shaft fits into the sleeve. The ultimate separation occurred on a crack plane inclined to the shaft axis which grew from a location at the junction of shaft and sleeve. Other cracks traversed nearly the entire cross-section on inclined planes to the axis (in opposed senses) bud did not completely sever. Examples are shown in Fgiures 5-10.

Surface damage was sustained on the completely separated (crack) surfaces and both the shaft and sleeve surfaces. All of this appeared to be after the failure damage. Damage on the shaft surface was confined to a region between some cracks but not others; rubbing on the sleeve surface was located about 180° opposite the shaft surface damage. Damage to the separated crack surface appeared to be due to impingement during shaft rotation after separation.

Cracks passing through the cross-section were separated by as much as 1 to 1-1/2 inch (measure of divergence) along the shaft axis. All these cracks are tied to a common feature, which is a longitudinal crack about 3/4-inch long located in one corner of the shaft keyway. This is illustrated in Figure 11.

The shaft was systematically forced to fracture through the cross-section along the existing nearly-through-shaft crack planes. Thus, major cracks associated with the extremities of the longitudinal crack were exposed. Further the stub of the shaft within the sleeve was removed for examination. These pieces are illustrated in Figure 12.

A rough fracture surface area was noted beside the keyway on the shaft section removed from the sleeve (arrow on Figure 12). A continuation of this fracture area was found after forcing the adjacent cracked area to complete separation. This is illustrated in Figures 13-15.

The fully exposed rough fracture surface area is seen to be derived from the longitudinal crack in the corner of the keyway. The plane of the rough fracture is parallel to and effectively an extension of the plane of the bottom of the keyway.

Several discrete fracture propagation systems were seen to extend from the extremities of the rough fracture area. These are all typified by smoother surfaces, by radial patterns and some "beach" markings. Arrows on Figures 9 and 15 show propagation patterns emanating from the keyway corner at the extremity of the rough fracture area on two of the major crack planes.

On other similar inclined fracture planes, similar fracture characteristics are observed.

FRACTOGRAPHY

A traverse across the fracture area illustrated in Figure 16 via Scanning Electron Microscope (SEM) revealed fracture characteristics shown in Figure 14. Three discrete fracture zones are noted: (1) flat surface in a narrow band immediately adjacent to the keyway corner, (2) microscopically rough angular surface extending about 1/2 to 3/4 inch from the keyway corner and (3) smooth surface initiating abruptly at the extremity of rough surface.

Figure 17 illustrates a portion of the locus of crack initiation at the corner of the keyway. Figures 18 and 19 illustrate details near the origin. Figure 20 shows the crystallographic character (looks "cleaved") which generally typifies the fracture surface at the origin.

Figures 21 and 22 show two different "beach" markings from a secondary propagation system. Figure 23 illustrates growth character preceding the last beach mark while Figure 24 illustrates growth character beyond the last beach mark (fast growth). Mixed mode conditions such as illustrated in Figure 25 were sometimes found near beach marks.

Sample bars were notched and hammer impacted at ambient temperatures to produce examples of high strain rate overload fractures. Fractographic examination showed that the surfaces generated were micro-dimpled (illustrated in

Figures 26 and 27); thus the material appeared relatively tough.

METALLOGRAPHY

Metallographic analysis showed that crack propagation was essentially transgranular with respect to both prior austenite and martensite grains. The pattern of propagation was observed to be typical of fatigue cracks. These points are illustrated in Figure 28.

DISCUSSION

PRIOR HISTORY

It has been found that Worthington does not have heat treat recorder charts to prove that the 17-4 PH material was heat treated to the desired H-1150 condition, prior to machining in their shops. Worthington has advised that their normal fabrication process was to 1) rough machine (including keyway), 2) heat treat, 3) final machine. Worthington records of material certifications and heat treat charts dated prior to 1971 have been discarded.

B&W did not, at the time of the order, invoke any special NDE or QA requirements on the shafts for the Decay Heat Pumps.

Material certifications have been located in B&W records. These show that material was supplied to Worthington from U. S. Steel Supply. The certification covers two pieces of 17-4 PH stainless steel in heat treat condition "A". Worthington ordered material as ASTM A564 Grade 630-Condition A-hot rolled.

MATERIAL CHARACTERISTICS

Chemical Composition

The chemical composition for the 17-4 PH stainless steel shaft is within limits of specification for ASTM A564 Grade 630, to which the material was ordered.

Tensile Properties

Tensile test data show that the alloy does not conform to typical H-1150 heat treatment properties for 17-4 PH steel. Yield stress values were 13 to 15% higher than expected and ultimate tensile stress 7 to 9% higher. Ductility

values were correspondingly lowered 25% and 14% for % elongation and % reduction of area in longitudinal tests, versus 47% and 66% respectively in transverse tests. Such anisotropy in ductility values is characteristic of the slightly tempered grades of 17-4 PH steel, but not H-1150.

Hardness Properties

Rockwell hardness values also indicate that the shaft has somewhat higher strength properties than are typical for the H-1150 treatment for 17-4 PH steel, i.e., R_c values as high as 35 versus 33 for H-1150.

Both tensile and hardness values appear to be more characteristic of a heat treatment approximating H-1025; transverse ductility values of the shaft are even lower than expected for H-1025.

Microstructure

The shaft microstructure is not typical for the H-1150 condition. The microstructure is more typical of a lesser tempering heat treatment, i.e., it contains finer dispersed copper particles and lesser prior austenite grain boundary decoration.

Reduced ductility in 17-4 PH stainless steel can be associated with excessive austenite grain growth, coarse martensite grain structure, and excessive delta-ferrite, as well as with the precipitation-hardened condition. However, none of the former three factors appear sufficiently abnormal to contribute substantially to the observed reduced ductility in tensile tests.

FAILURE CHARACTERISTICS

It appears that cracking initiated at the corner of the keyway on a lineal locus along the shaft axis. The initial crack extension proceeded by a transgranular mechanism. There were slight tear ridges oriented perpendicular to the corner of the keyway which suggested that a planar crack front moved away from the corner.

The initial crack growth is most consistent with a fatigue propagation mechanism. Initial crack growth character is not consistent with impact fracture as determined in lab tests. Stress corrosion cracking similarly is not consistent with the observed fracture character-stress corrosion should proceed intergranularly in a decay heat pump shaft environment. However, if chlorides are present, then the crack propagation could be transgranular. No material deficiencies or surface flaws that might have initiated cracking were found in the area of the crack origin.

Crack extension beyond the initial region proceeded by a structure-sensitive ("cleaved") micro-topology which is characteristic of fatigue propagation for many materials in the realm of low stress intensity range associated with crack propagation rates less than 10^{-6} inches per cycle.

After the initial crack extended about 1/2 to 3/4-inch, it appears that a critical size was reached, after which the fatigue process assumed somewhat different, more classical (beach marked), fatigue character.

Some bands of intergranular fracture mixed with transgranular fracture were observed. This suggests possible grain boundary weakness in the material or some environmental effect on propagation. Either phenomenon would seem to be incidental and not significant to the failure process.

FAILURE CAUSES

The inclination of crack planes to the shaft axis suggests that maximum tensile stresses in torsional loading are associated with the failure and crack propagation.

It appears that the crack initiated at the corner of the keyway in a classic "peeling" mode because the operating stresses were intensified by the square corner of the keyway. Stress intensification by a factor of five (5) or more is not unreasonable for this geometry. The Armco blue book for 17-4 PH stainless steel lists a fatigue life of 280×10^6 cycles at 83 ksi for the H-1150 condition. The actual life of the shaft was about 85×10^6 cycles. This is somewhat between the expected life for the H-1150 and H-900 conditions for a

stress around 80 ksi (for H-900 at 82 ksi, the life is 41 x 10^6 cycles). Based on tensile and metallography data, the actual heat treatment of the shaft appears to place it somewhere between the H-900 and H-1150 conditions. The lesser tempered conditions exhibit reduced fatigue life.

Design of the keyway appears to lie at the root of the problem. Figure 29 illustrates the total lack of fillet in the keyway corner profile.

Based on our examination, the questionable heat treatment and the non-filleted keyway are the metallurgical factors that led to the failure of the Crystal River III Decay Heat Pump Shaft.

L. W. Sarver

J. S. Rovder

whm

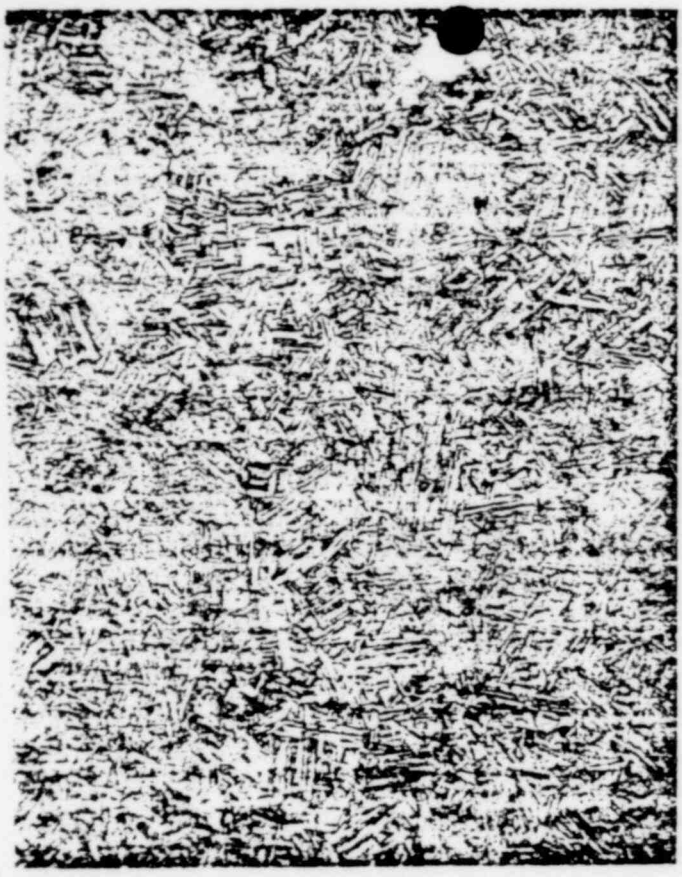

100X

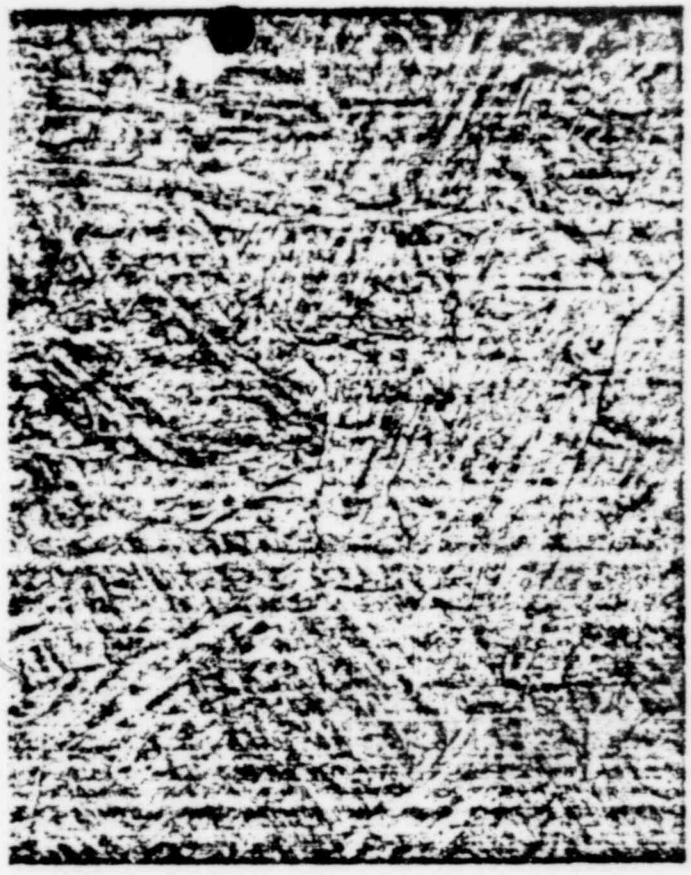

500X

1100X

Figure 1. Photomicrographs showing the microstructure in a transverse section near the shaft center.

HCl - Picric Acid Etch.

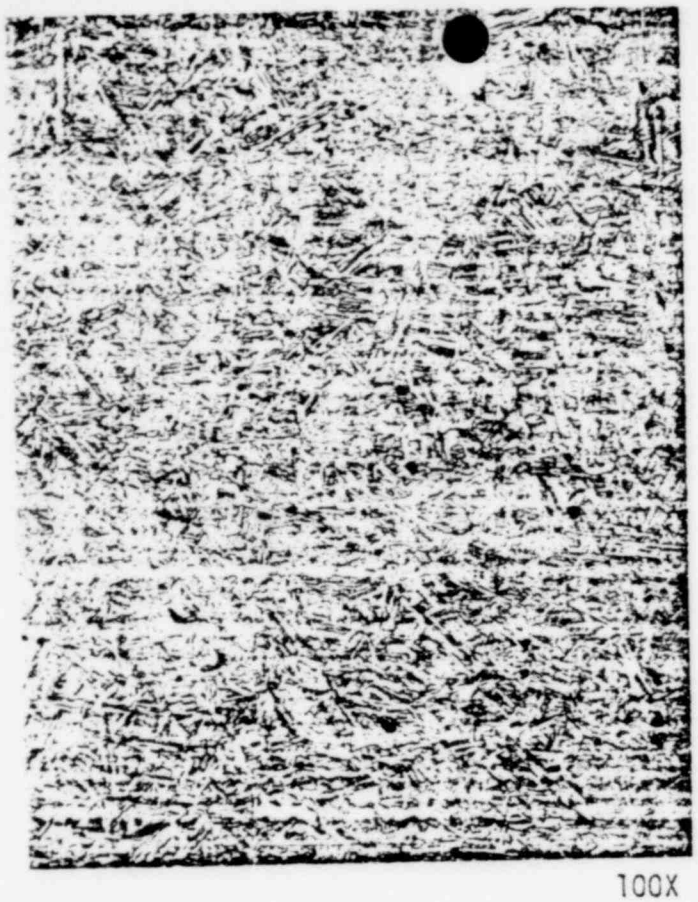

100X

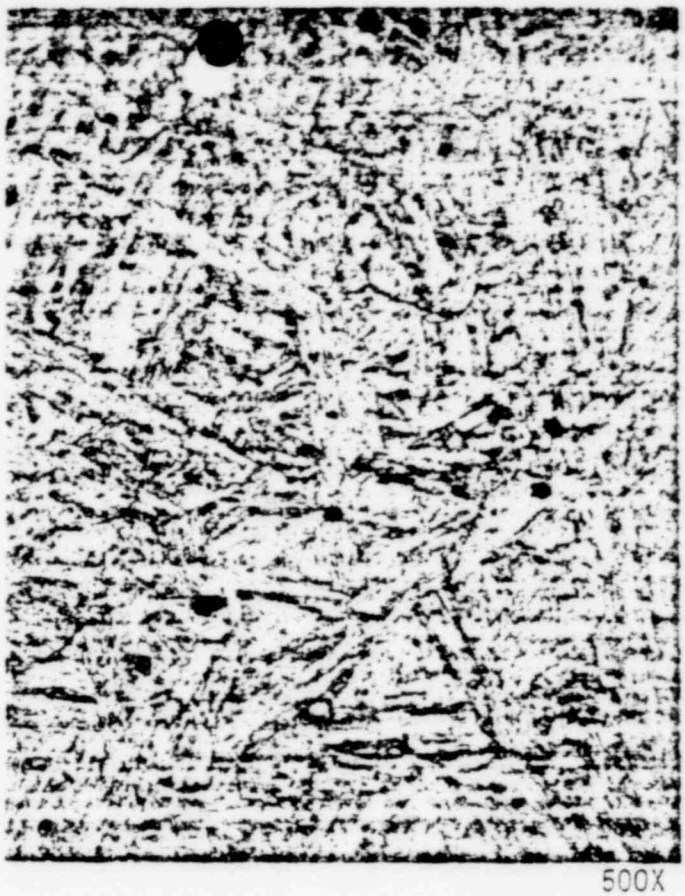

500X

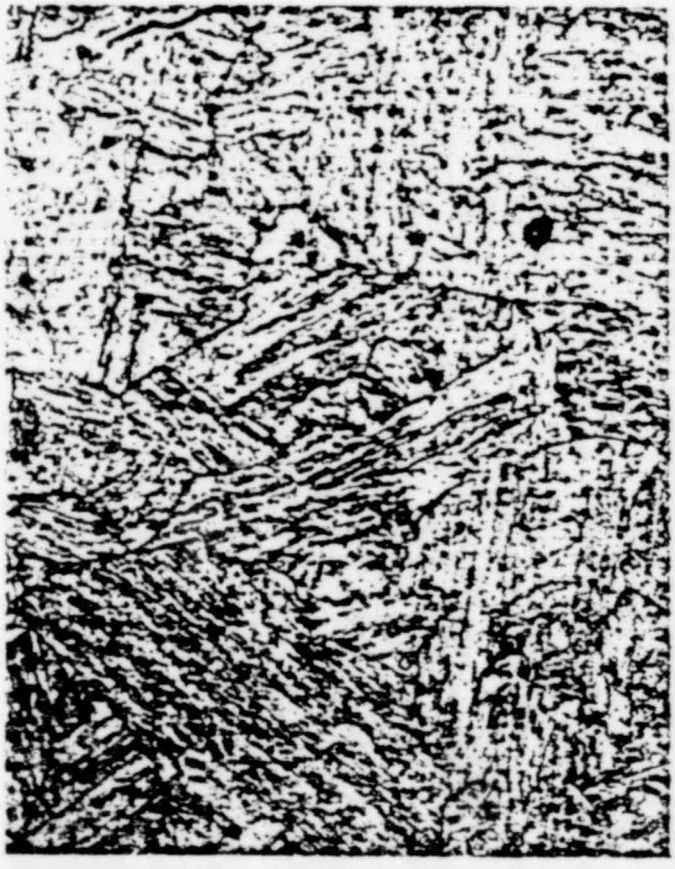

1100X

Figure 2. Photomicrographs showing the microstructure in a transverse section near the shaft OD.

100X

500X

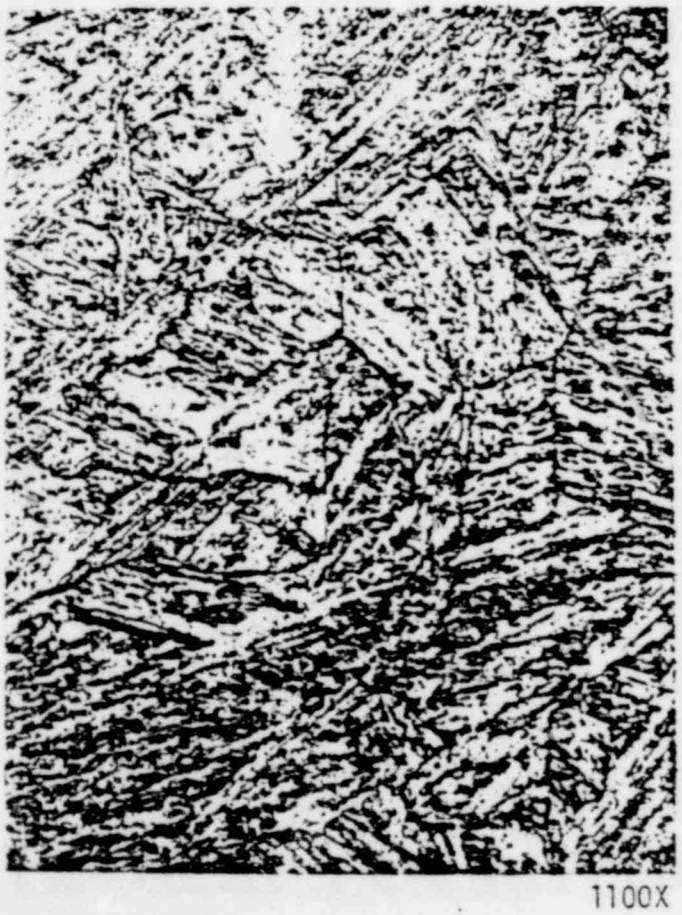

1100X

Figure 3. Photomicrographs showing the microstructure in a longitudinal section near the shaft center.

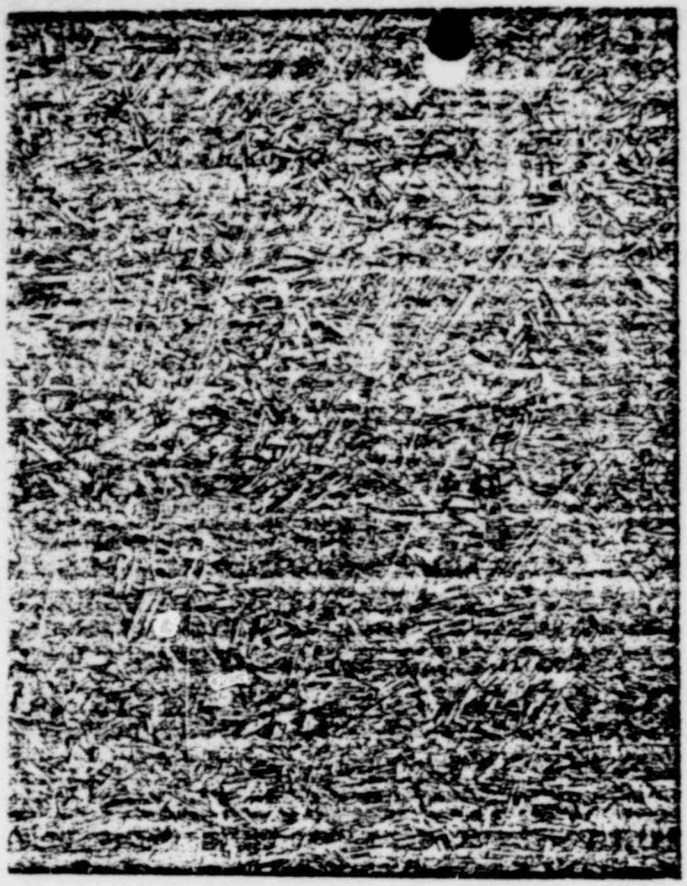

100X

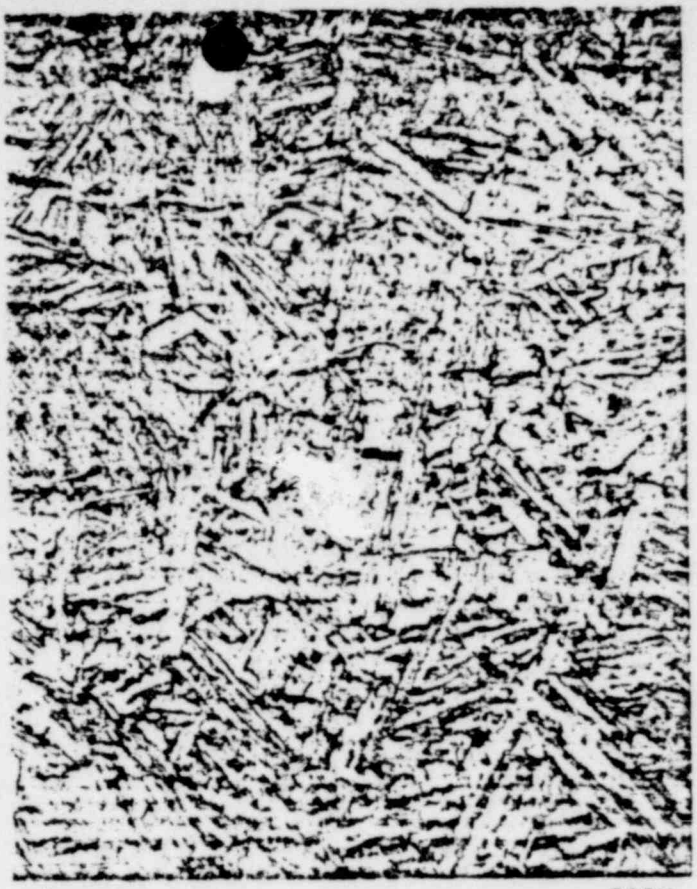

500X

1100X

Figure 4. Photomicrographs showing the microstructure in a longitudinal section near the shaft OD.

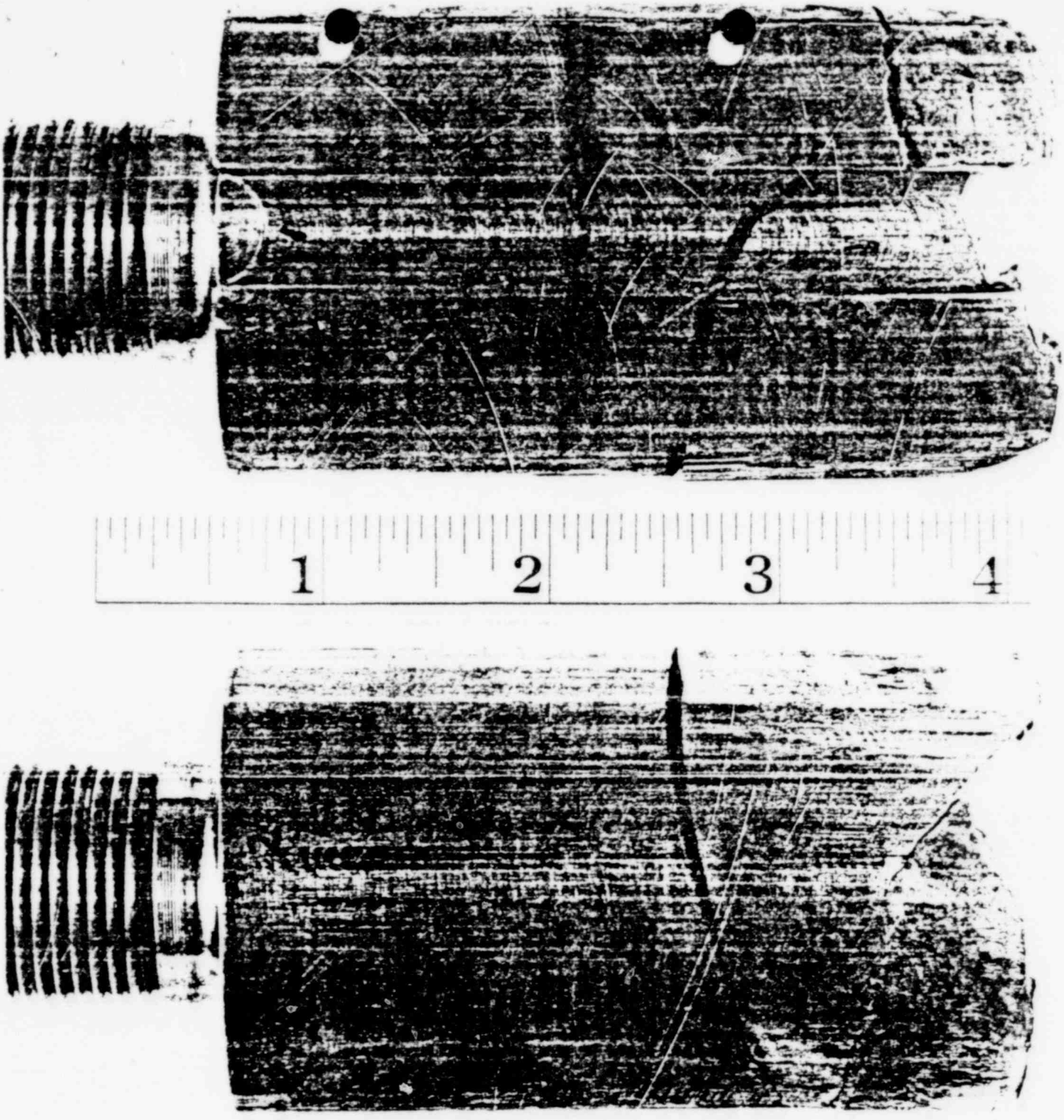

Figure 5. Photomacrograph of fractured shaft, 1. at key way and 2. rotated 90°.

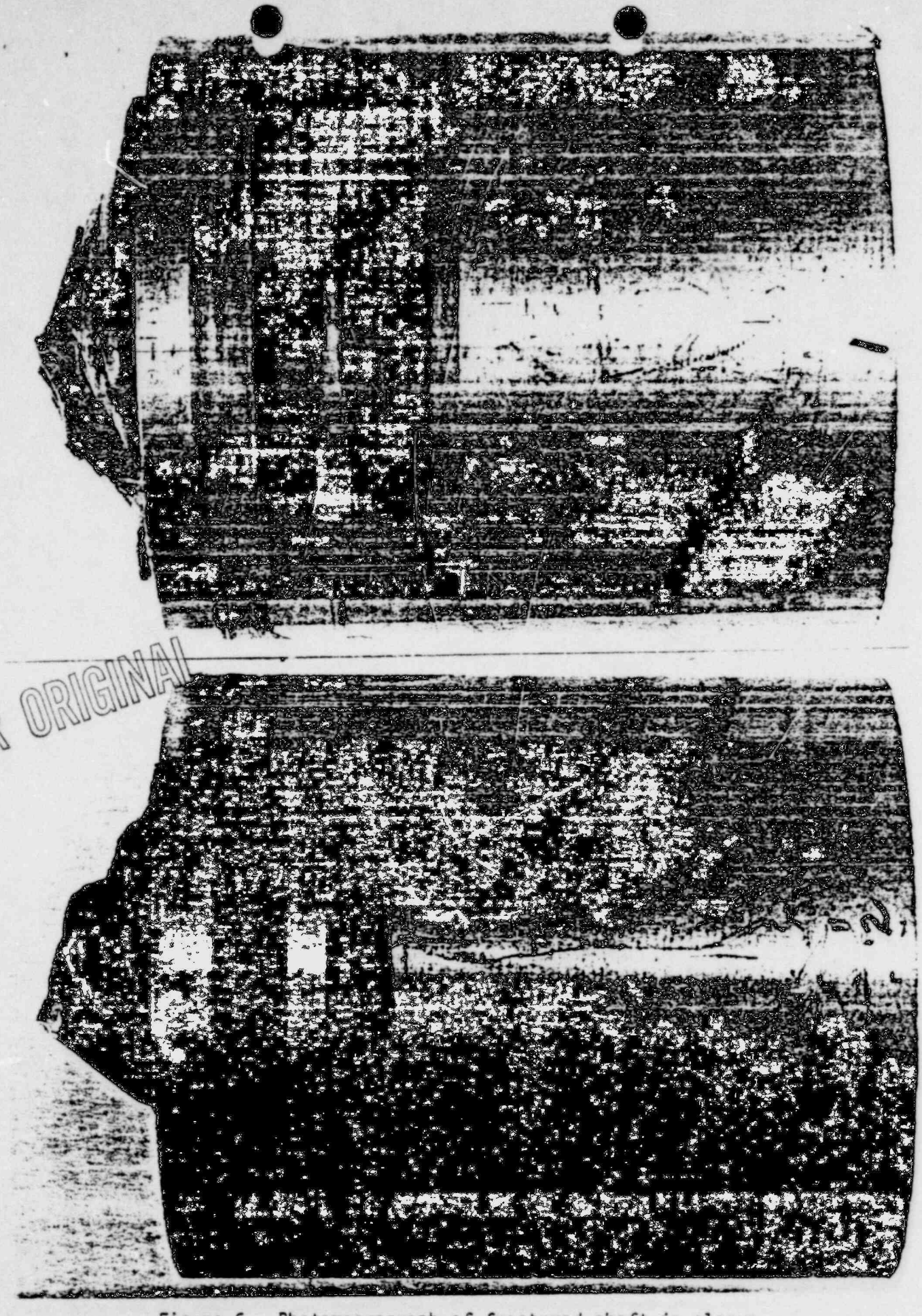

Figure 6. Photomacrograph of fractured shaft in sleeve, 1. at keyway and 2. rotated 90°.

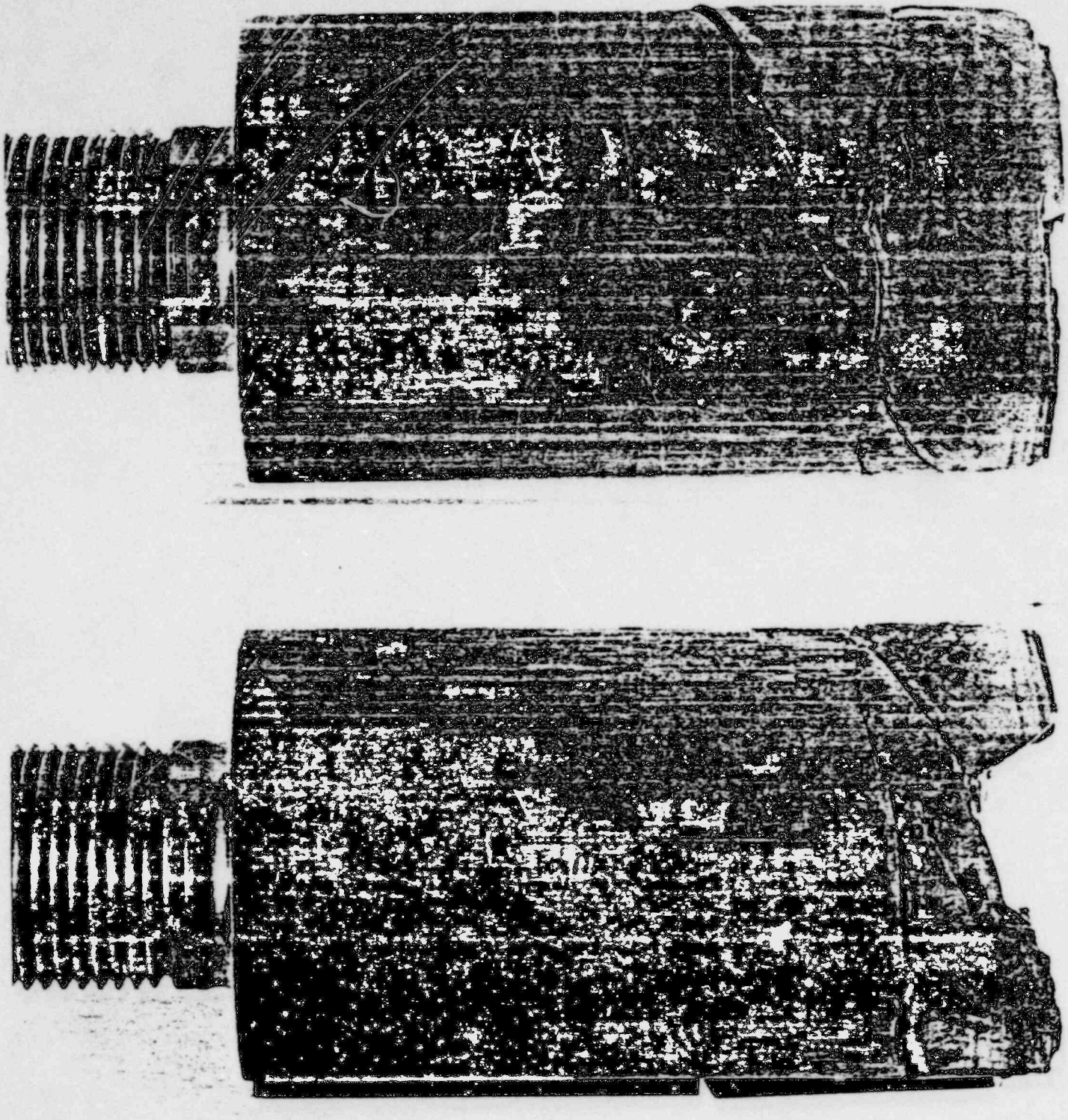

Figure 7. Photomacrographs of fractured shaft rotated 180° (3) and 270° (4) with respect to keyway.

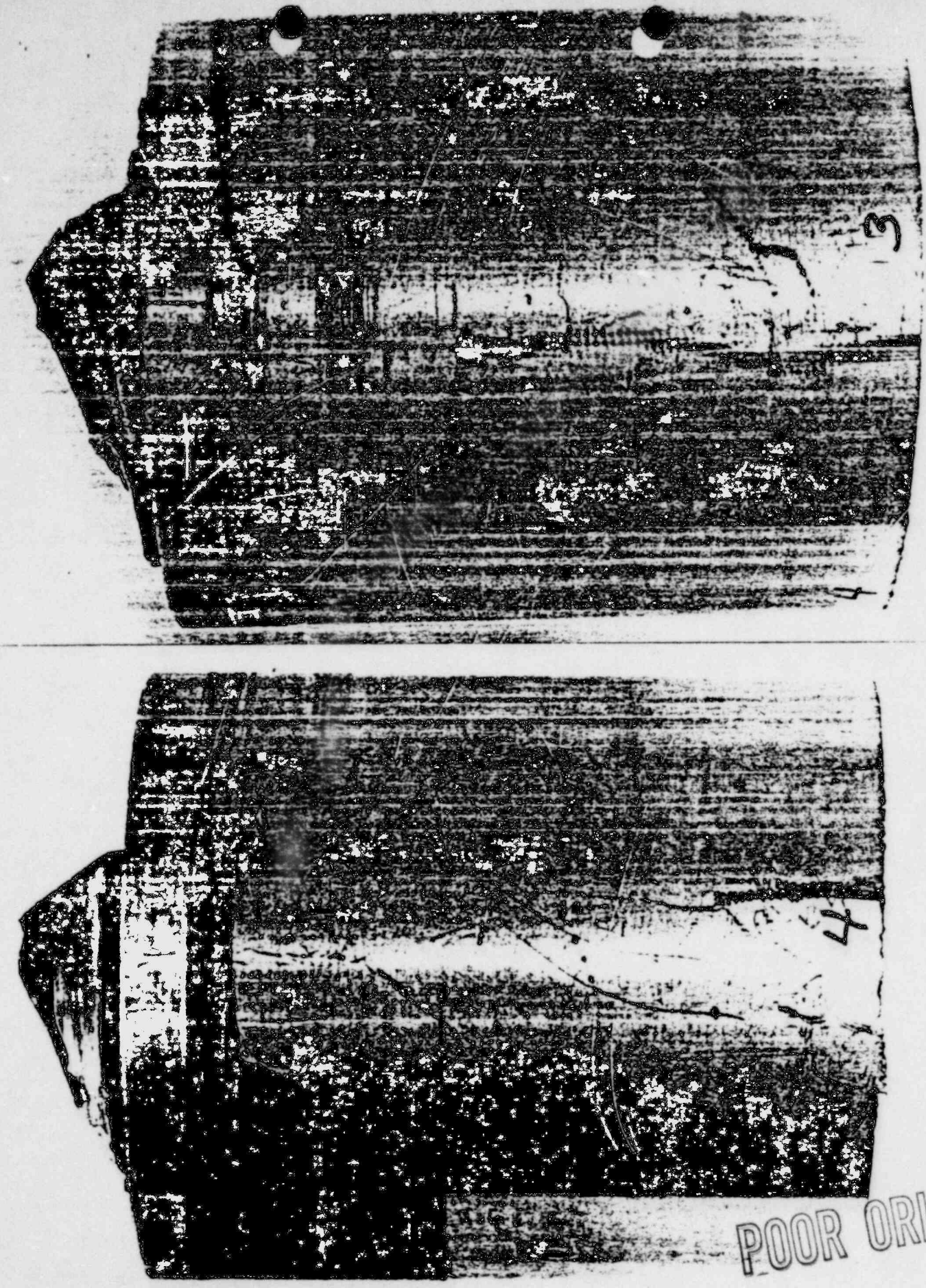

Figure 8. Photomacrograph of fractured shaft in sleeve rotated 180° (3) and 270° (4) with respect to keyway.

Figure 9. Photomacrograph of fracture plane on shaft. Arrow indicates bench marks.

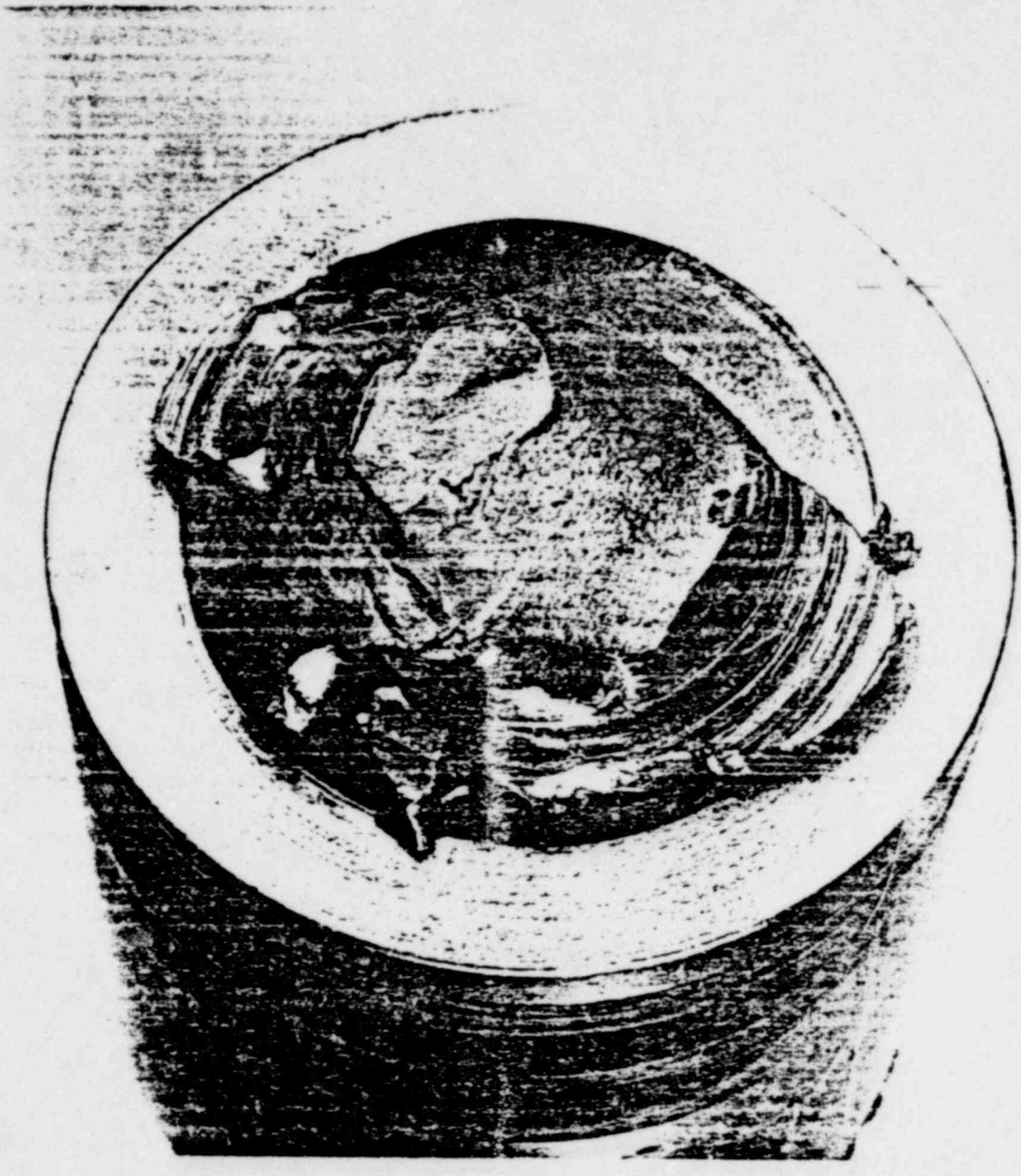

Figure 10. Photomacrograph of fracture plane on shaft. Matching surface to fracture plane shown in Figure 9.

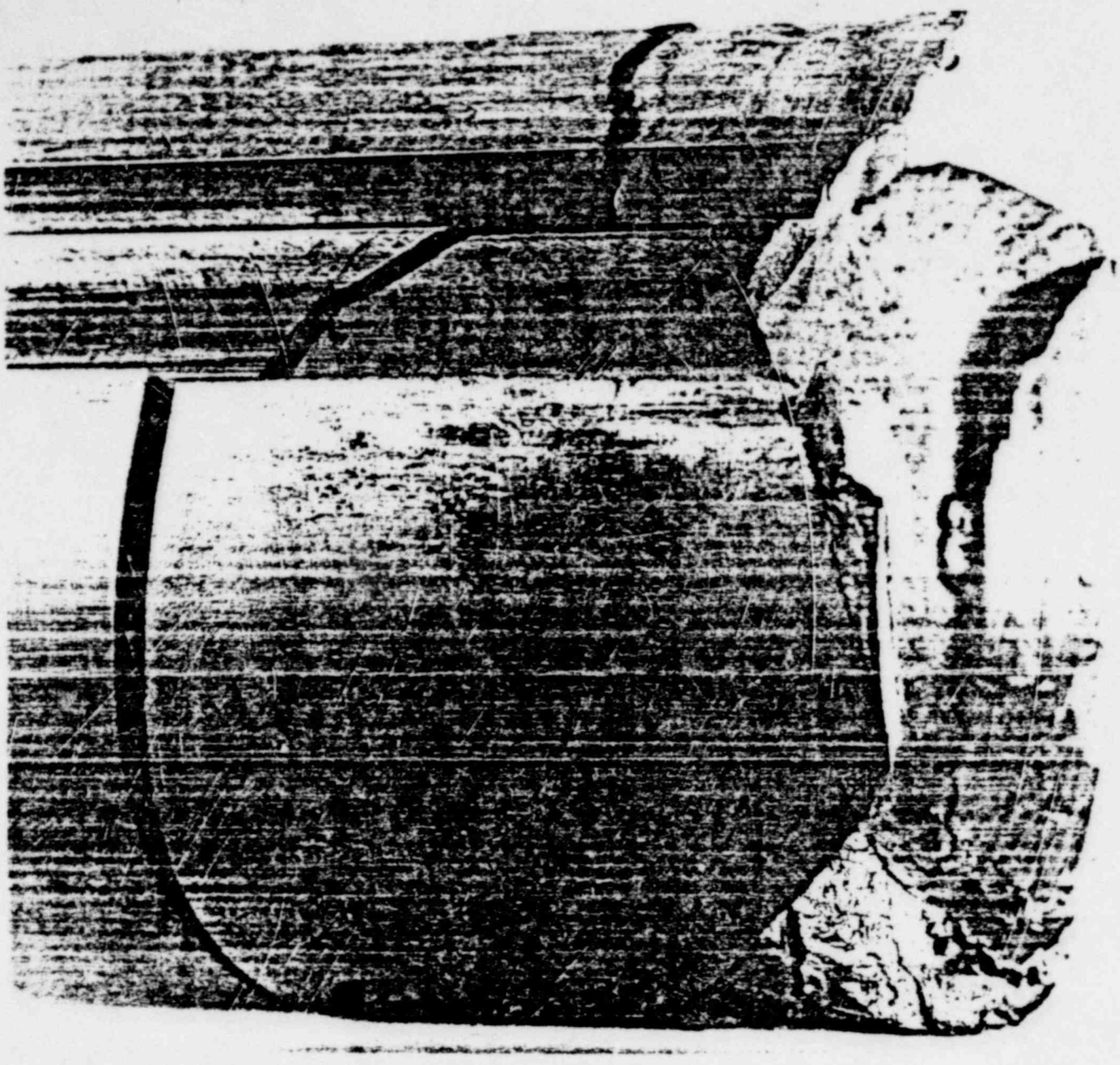

Figure 11. Photomacrograph showing longitudinal crack in keyway corner.

fhis
acture
plane
own in
gure 15.

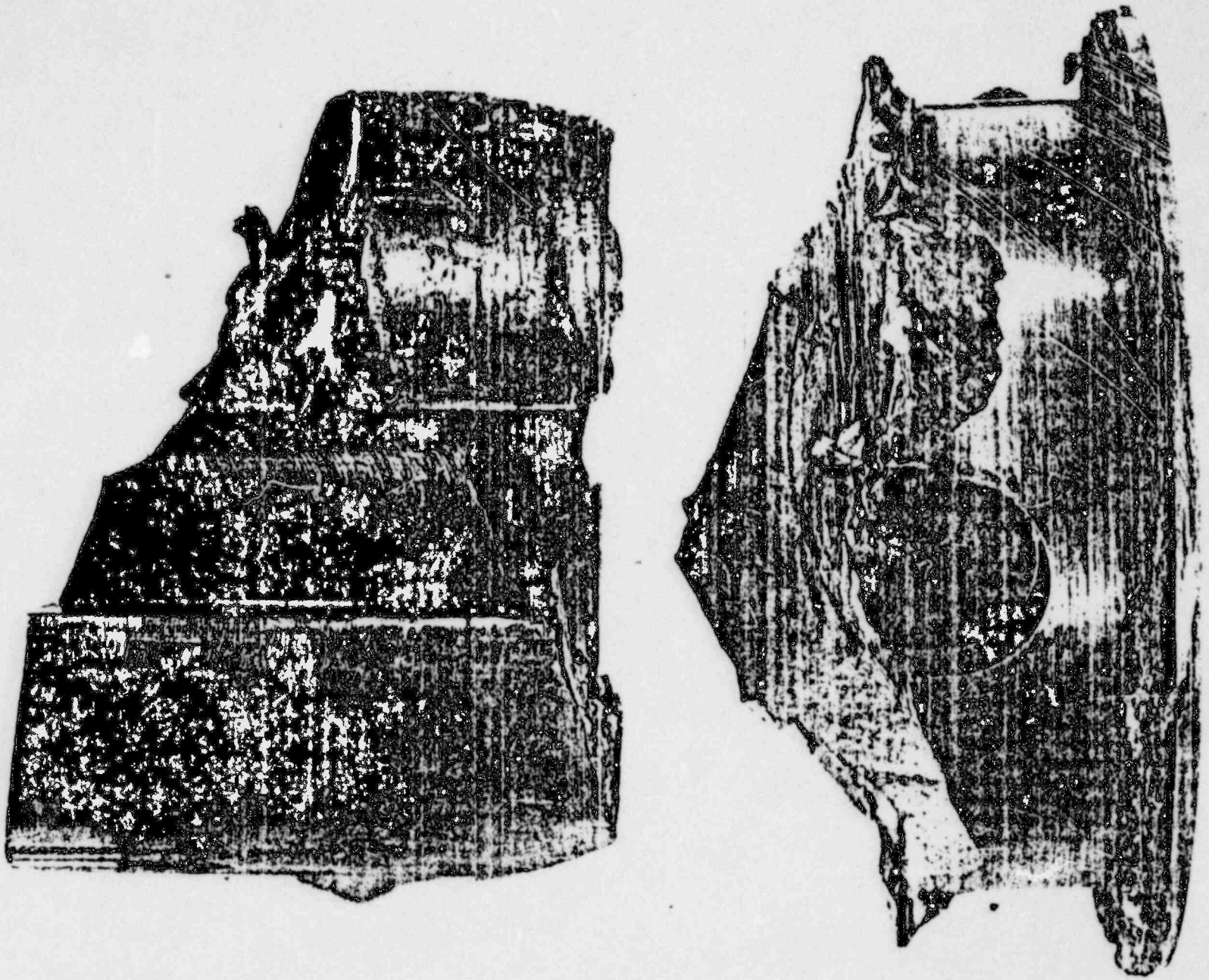

Figure 12. Photomicrograph showing shaft removed from sleeve (section on the right) and adjacent crack forced to complete separation (section on the left).

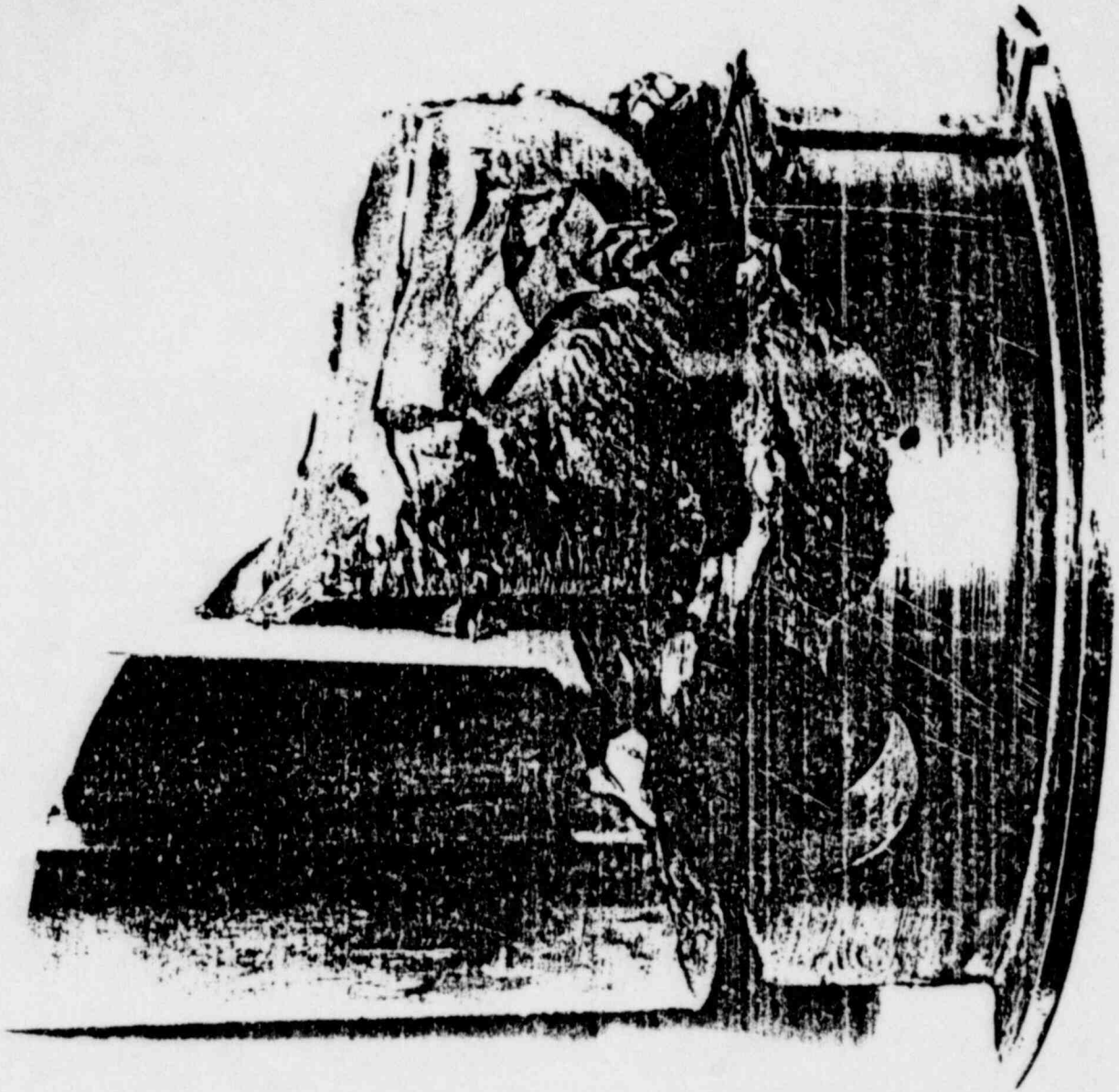

Figure 13. Photomacrograph showing the same sections as in Figure 12 with section A removed.

Figure 14. Photomacrograph showing the reconstruction of the shaft after forcing partial separations to completion.

Figure 15. Photomacrograph showing the fracture plane forced to complete separation. Location of plane shown on Figure 12.

Figure 16. A series of scanning electron microscope photomicrographs traversing piece A in Figure 14.

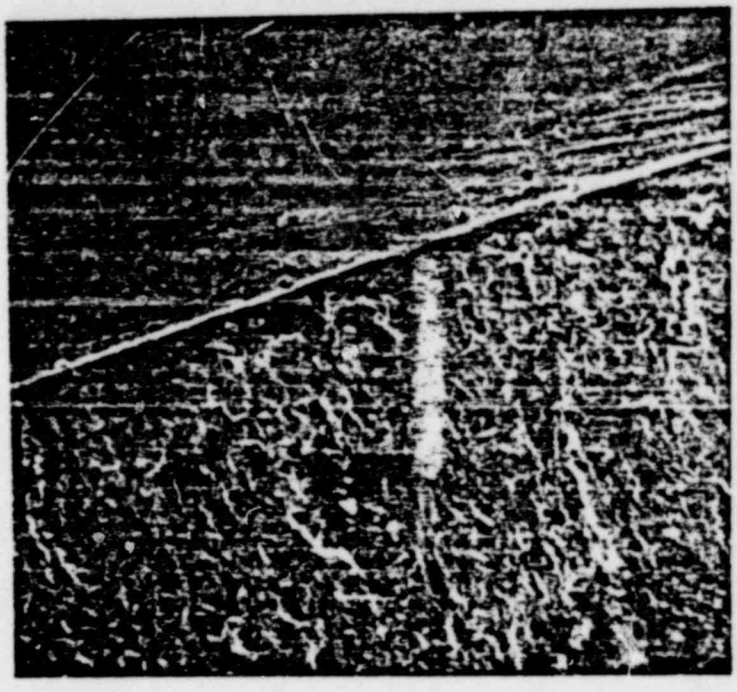

62X

Figure 17. Fractograph showing portion of locus of crack initiation (corner of keyway).

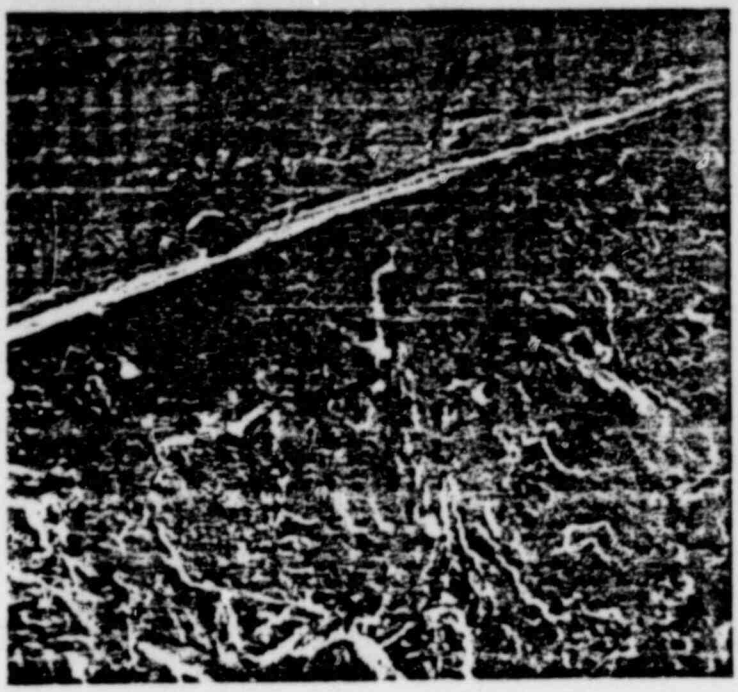

190X

Figure 18. Fractograph of crack origin in corner of keyway.

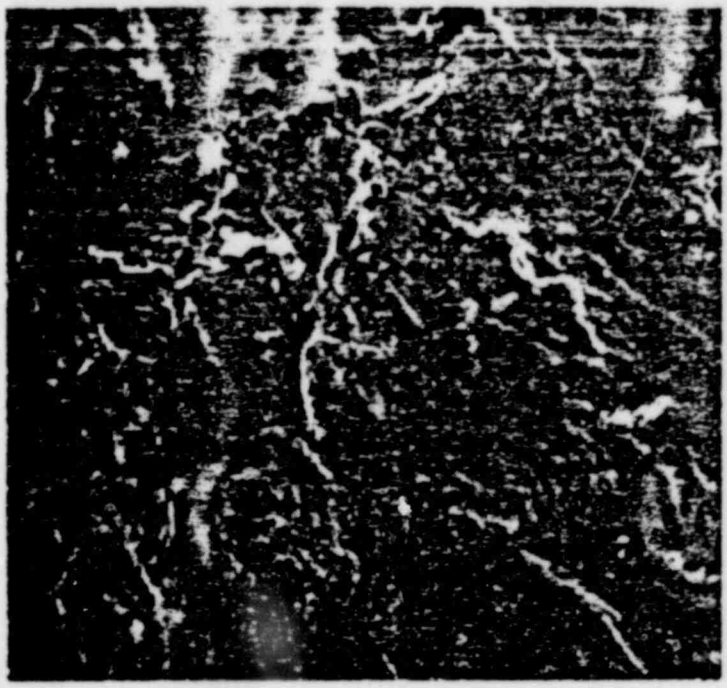

620X

Figure 19. Fractograph of detail in crack origin area.

1400X

Figure 20. Fractograph showing detail in crystallographic ("rough") fracture surface area.

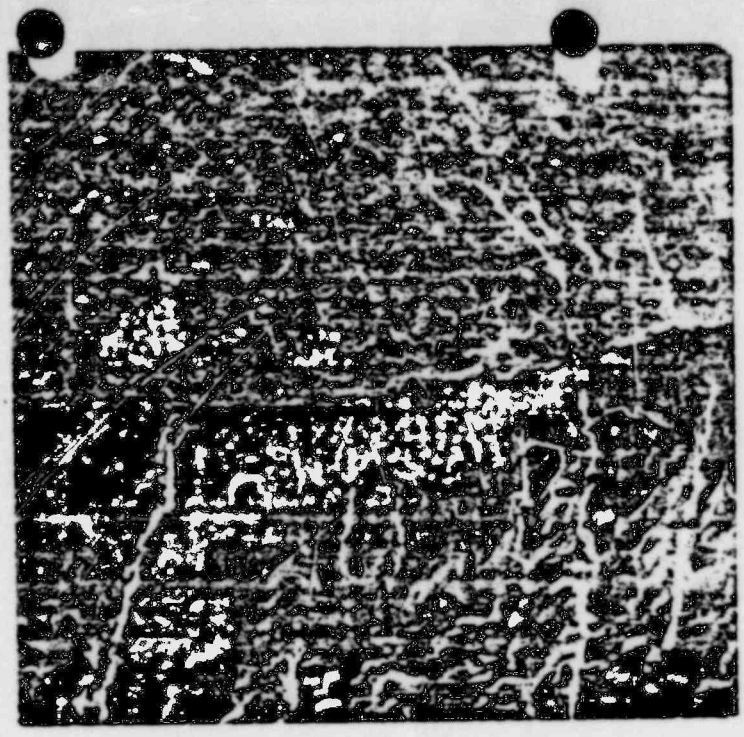

50X

Figure 21. Fractograph of beach mark in secondary crack propagation system.

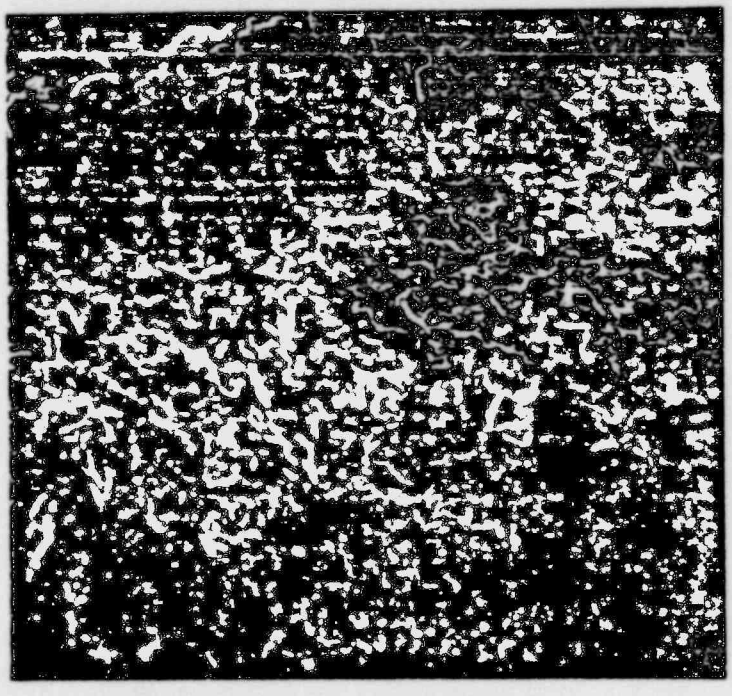

50X

Figure 22. Fractograph of beach mark in secondary crack propagation system. Mixed mode fracture is present in the mid-region of the photo.

500X

Figure 23. Fractograph showing crack growth character preceding beach mark in secondary propagation system.

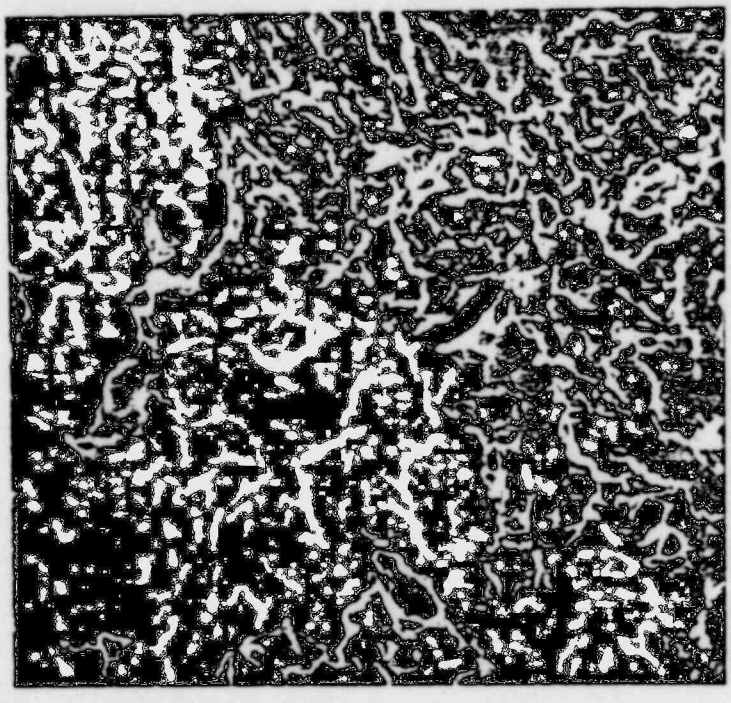

500X

Figure 24. Fractograph showing crack growth character beyond last beach mark in a secondary propagation system.

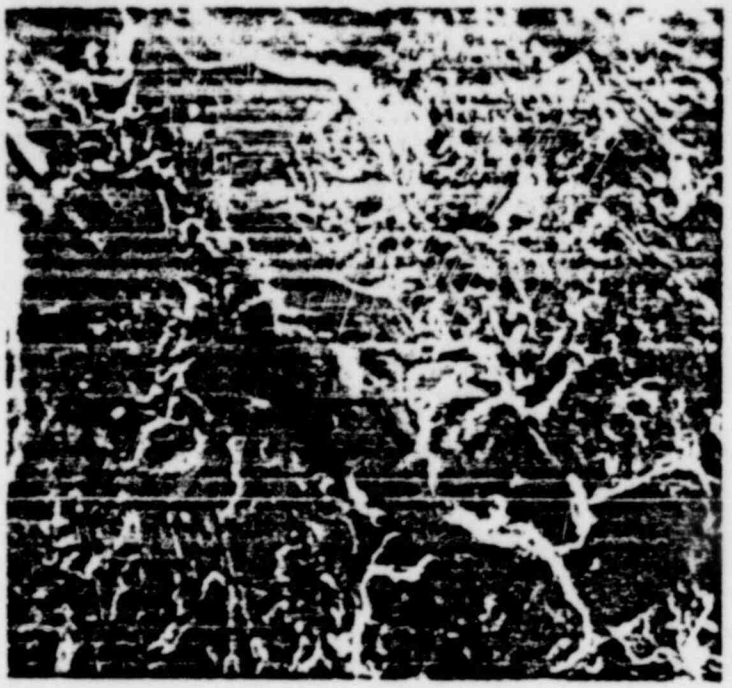

500X

Figure 25. Fractograph showing detail of mixed mode fracture character near beach marks.

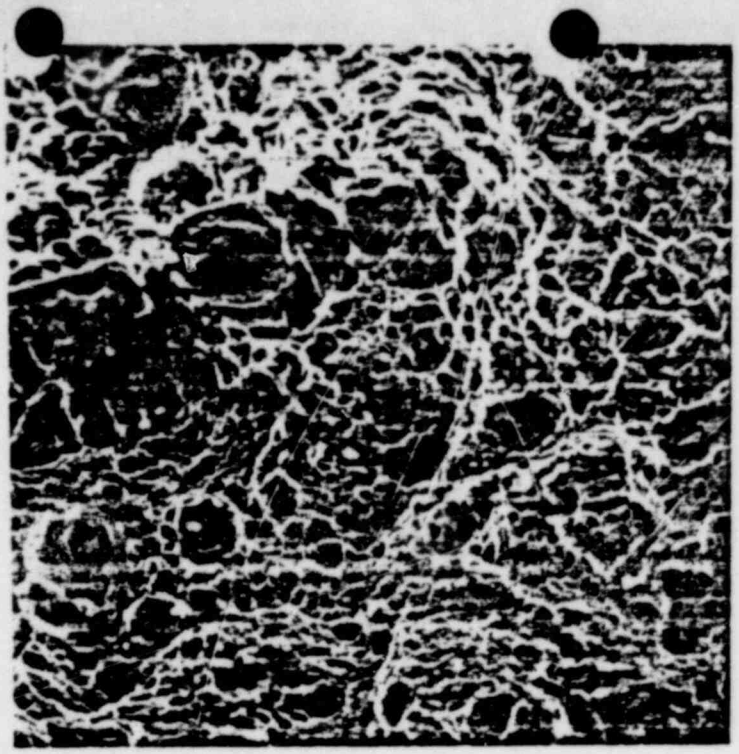

Figure 26. Crack Surface Perpendicular to Shaft Axis 550X

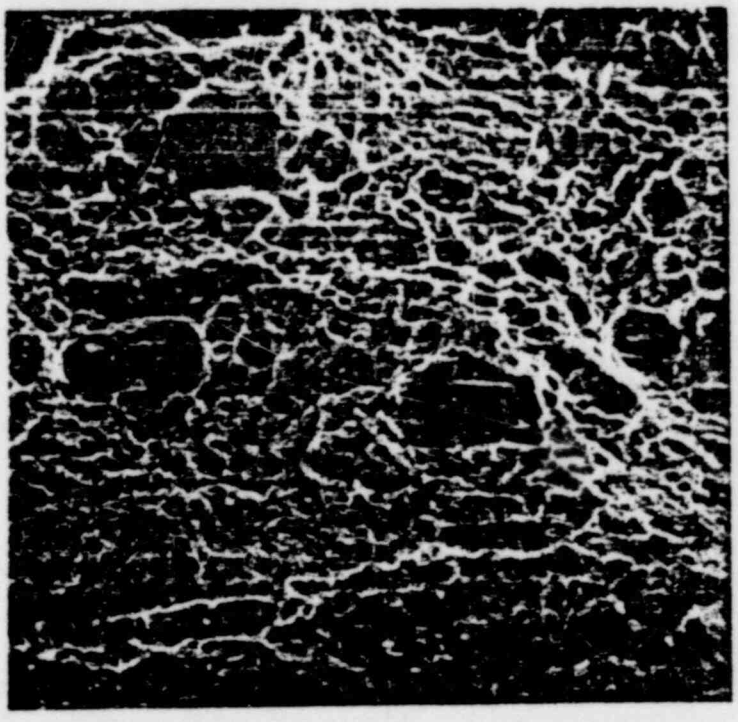

Figure 27. Crack Surface Parellel to Shaft Axis. 550X

Appearance of Fracture Surfaces Generated by Impacting Saw-Notched Rectangular Bars of the 17-4 PH Shaft Material.

Transverse Plane 10X

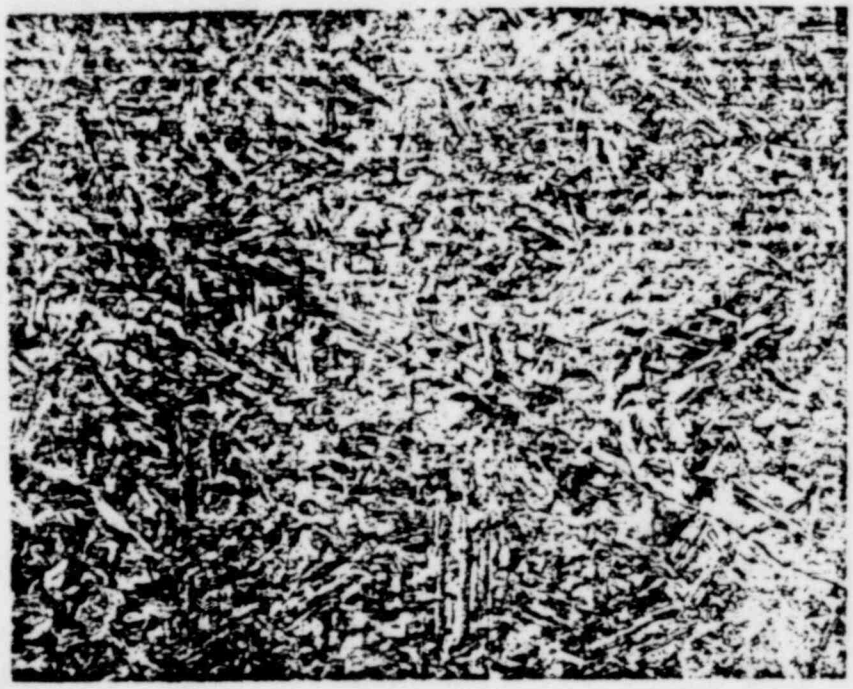

Longitudinal Plane 150X

Figure 28. Optical Photomicrographs Illustrating Microstructural Crack Profiles

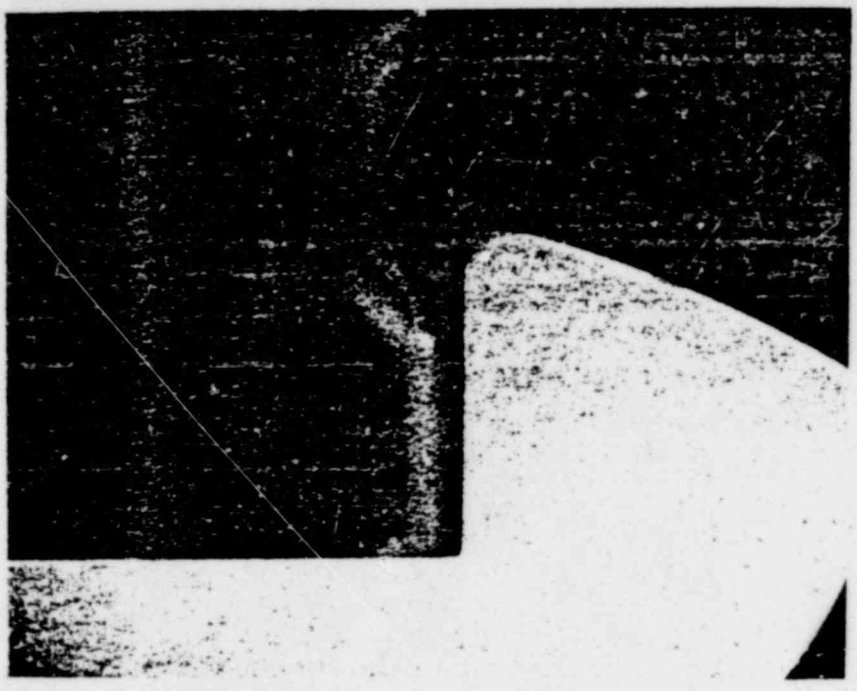

7X

Figure 29. Optical photomacrograph showing the profile of the keyway. Note the absence of fillet in the keyway corner.